



## ORIGINAL ARTICLE

# Ice-templated porous polymer/UiO-66 monolith for Congo Red adsorptive removal



Lang Wen<sup>a</sup>, Xuedan Chen<sup>a,b</sup>, Chao Chen<sup>a</sup>, Ruisong Yang<sup>a,b</sup>, Min Gong<sup>a,b</sup>,  
Yiguo Zhang<sup>c</sup>, Qingshan Fu<sup>a,b,\*</sup>

<sup>a</sup> College of Material Science and Engineering, Sichuan University of Science and Engineering, Zigong 643000, China

<sup>b</sup> Key Laboratory of Material Corrosion and Protection of Sichuan Province, Zigong 643000, China

<sup>c</sup> Yuxing carbon production company limited, Zigong 643000, China

Received 14 December 2019; accepted 5 April 2020

Available online 13 April 2020

## KEYWORDS

Water treatment;  
UiO-66;  
Adsorption;  
Congo Red;  
Ice templating;  
Cross-linking

**Abstract** Chitosan/MOF composite porous monolith used in water remediation as adsorbent can realize high-efficient removal of pollutant in water and facile recycling from water. However, dissolution of chitosan (without crosslinking) in acidic aqueous solution will cause breakage of composite monolith. Herein, we report a chitosan/UiO-66 monolith prepared by ice-templating method. Specially, a pre-crosslinking treatment (by glutaraldehyde) is employed before the monolith formation, which obviously boosts its stability in aqueous solution. The composite monolith is evaluated by SEM, N<sub>2</sub> adsorption, XRD, and batch adsorption tests for Congo Red (CR). The results show that the composite monolith possesses a typical ice-templating structure with hierarchical (micro- / meso- and macro-) pores. UiO-66 particles are embedded on the surface of chitosan matrix, and the crystal structure of UiO-66 is not changed obviously by the crosslinking and freezing process. The composite monolith exhibits high adsorption efficiency (90% of CR was removed from its aqueous solution in 60 min) and the maximum adsorption capacity of 246.21 mg/g (derived from Langmuir model) can be reached. After adsorption, the monolith is collected by a facile procedure and recovered using ethanol for evaluating its reusability. After 4 cycles, the CR removal efficiency of the composite monolith still remains ~90% of the initial efficiency. This work demonstrates that the simple crosslinking procedure before monolith formation can ensure the intact shape of the chitosan/MOF monolith during adsorption.

© 2020 The Authors. Published by Elsevier B.V. on behalf of King Saud University. This is an open access article under the CC BY-NC-ND license (<http://creativecommons.org/licenses/by-nc-nd/4.0/>).

\* Corresponding author at: College of Material Science and Engineering, Sichuan University of Science and Engineering, Zigong 643000, China.

E-mail address: [sendysan@suse.edu.cn](mailto:sendysan@suse.edu.cn) (Q. Fu).

Peer review under responsibility of King Saud University.



## 1. Introduction

Depletion of global clean water has become a big crisis to all mankind. Kinds of pollutants, such as heavy metal ions and organic dyes, are causing heavy pollution of water. Different routes have also been developed to relieve this crisis (Huang

et al., 2018; Xue et al., 2018; Han et al., 2018; Salleh et al., 2011).

In the case of organic dyes, most of them may cause harmful to human and animal health due to their being toxic, mutagenic, carcinogenic (Bulut et al., 2008; Salleh et al., 2011). For example, Congo red (CR), one azo dye, could be metabolized into benzidine, which is linked to cancer of the human bladder (Puvaneswari et al., 2006; Shetti et al., 2019). CR also leads to decrease of serum protein concentration, platelet aggregation, thrombocytopenia, disseminated microembolism (Frid et al., 2007), and some allergic reactions (Puvaneswari et al., 2006; Chakraborty et al., 2003; Chatterjee et al., 2009; Chen et al., 2014). As such, it is really emergent to effectively remove some morbidic dyes from water (Bhatt et al., 2012; Chen et al., 2015). So far, there are many ways to treat dye-contained wastewater, including adsorption (Tian et al., 2018; Beheshti et al., 2018), flocculation (Mittal et al., 2018; Kalantari et al., 2018; Zhao et al., 2018a,b), electrolysis (Fu and Jian, 2016) and biodegradation (Gupta et al., 2013). Among them, the adsorption is an attractive and widely used method in the purification of dye-contained wastewater due to its high adsorption efficiency, easy operation and low cost (Gupta et al., 2013).

For the adsorption method, choosing suitable adsorbents plays a critical role for removal of target contaminations. Metal-organic frameworks (MOFs) are a new family of microporous materials consisting of metal clusters interconnected by organic ligands centered on transition elements (Ahmed and Jung, 2014; Maurin et al., 2017). One of the most important properties of MOFs is their precisely defined apertures (from a few angstroms to a few nanometers) that can be controlled in a large range to allow size and shape selectivity toward guest species (Zhao et al., 2018a,b). Meanwhile, kinds of functional sites can be easily introduced on the framework, cavities and channels of MOFs for special applications (Park et al., 2012; He et al., 2013; Lin et al., 2016; Ahmed and Jung, 2014; Chen et al., 2015).

Given these advantages, several MOFs have been employed for adsorption of contaminants from wastewater, (Ahmed et al., 2017; Li et al., 2016; Kumar et al., 2016; Han et al., 2018) such as MIL-Ti (adsorptive capacity of 1296 mg/g for Basic Red 46, and 1257 mg/g for Basic Blue 41, 862 mg/g for Methylene Blue (MB)) (Oveisi et al., 2017), Er-MOF (removing 92% of MB from wastewater) (Mohammadnejad et al., 2017) and UiO-66-NH<sub>2</sub> with high adsorptive capacity for MB (555.6 mg/g) (Lv et al., 2019). Specially, for removal of CR from water, UiO-66 exhibits the adsorption capacity of ~ 280 mg/g (Han et al., 2017) and ZIF-8 yields a really high adsorptive capacity of 798.0 mg/g (Fan et al., 2017). Furthermore, fabrication of MOF/polymer or MOF/carbon composites can boost the adsorption capacity obviously. For example, graphene oxide/metal-organic frameworks (GO/MOFs) can reach a removal capacity of 2489 mg/g for CR from aqueous (Du et al., 2019).

The use of MOF nanoparticles for remediation of water (involving liquid phase) can enhance mass transport due to high external surface area (Seo et al., 2015). However, this procedure causes the difficulty in collecting MOF nanoparticles after adsorption removal, which is usually performed by centrifugation or infiltration with nanoporous membranes (Ma et al., 2017). To address this issue, MOF monoliths (Lim et al., 2019) or MOF/polymer composites (Kalaj et al., 2019) have been prepared by kinds of ways, such as electrospinning

(Duan et al., 2019), ice templating (Fu et al., 2017). Ice-templating is a highly versatile and efficient process to make a wide range of porous materials, including polymer, ceramics, and composites (Roleček et al., 2019; Suresh and Kumaraswamy, 2019; Fu et al., 2019). The resultant materials exhibit highly interconnected ice-templating macropores and contain porosity/properties contributed by nanoparticles and polymers in the materials (Lai et al., 2018; Deville, 2018). In our previous work, we fabricated a 3D porous polymer/MOF (chitosan/UiO-66) composite monolith using ice-templating and subsequent soaking in basic solution (for neutralizing residual acetic acid in chitosan, avoiding dissolution of chitosan monolith in water). This monolith was used for MCPP adsorptive separation from water and showed a high removal capability (Fu et al., 2017). However, alkaline solution caused the breakdown of UiO-66 crystal structure, leading to a sharp drop in special area surface. As such, in this work we substituted soaking in basic solution for chemical cross-linking by glutaraldehyde. The process of chemical cross-linking can ensure the intact figuration of the composite monolith and do not break crystal structure of UiO-66 at the same time. The adsorptive capacity for CR by the cross-linked chitosan/UiO-66 monolith was evaluated and adsorption isotherm, kinetic, influence of pH and recycling performance were studied as well.

## 2. Experimental section

### 2.1. Materials

Chitosan (<200 MPa·S), Zirconium chloride (ZrCl<sub>4</sub>) and benzene-1,4-dicarboxylate (H<sub>2</sub>BDC) were purchased from Macklin Biochemical Co., Ltd. (Shanghai, China). Glutaraldehyde (GLA, 50 wt%), acetic acid (HAc, 36 wt%), hydrochloric acid (HCl, 36 wt%), benzoic acid (BA) and N, N-Dimethylformamide (DMF) were bought from Aladdin Chemistry Co., Ltd. (Shanghai, China). Ultrapure water prepared using Milli Q system was used during this work. All of the reagents were used as received without further purification.

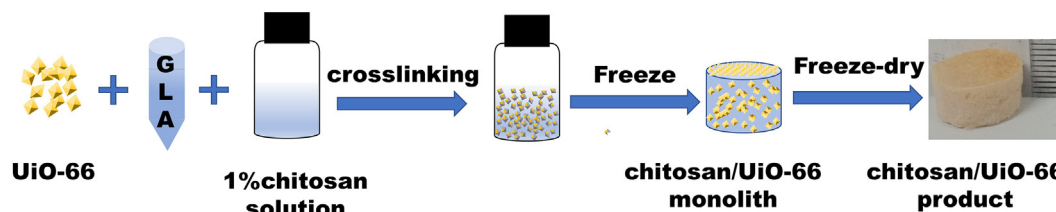
### 2.2. Preparation of adsorbent

#### 2.2.1. Synthesis of UiO-66

ZrCl<sub>4</sub> (2 mmol), BDC (2 mmol), benzoic acid (20 mmol), and HCl (36 wt%, 4 mmol) were dissolved into DMF (36 mL) with ultrasonic treatment for 10 min in a conical flask, covered with aluminum foil. The mixture was heated at 120 °C for 48 h, and white powder happens. The white powder of UiO-66 nanoparticles was collected by centrifugation and washed three times with DMF at room temperature.

#### 2.2.2. Preparation of composite monolith

In this work, chitosan/UiO-66 composite monolith was prepared by combination of crosslinking & ice-templating as shown in Scheme 1. First, 1 wt% chitosan solution was prepared by dissolving 0.4 g chitosan powder in 39.56 mL 2 wt% HAc aqueous solution ( $\rho_{2 \text{ wt\% HAc}} \approx 1.001 \text{ g/cm}^3$ , prepared by diluting 36 wt% HAc with ultrapure water). Then 0.1 g UiO-66 plus 0.8 mL 5 wt% GLA (50 wt% GLA was diluted ten times using ultrapure water) were added to the 1 wt%



Scheme 1 Procedure for formation of chitosan/UiO-66 monolith.

chitosan solution (10 mL), with stirring at 60 °C. After 1 h, a light-yellow suspension was acquired. The suspension was transported into glass bottles (with the size of  $\Phi 16$  mm  $\times$  33 mm, 1 mL per bottle), and the bottles were frozen at  $-20$  °C for 12 h in a refrigerator. Then, the frozen samples were transferred into a freeze-dryer (SCIENTZ-12 N, Zhejiang, China) and freeze-dried for 24 h to form chitosan/UiO-66 monoliths. The monoliths were washed with deionized water and acetone in sequence (6 times every solution, 15 min every time) to remove residual acetic acid, and then soaked in cyclohexane for 4 h before air-drying in a fume hood. The resultant monolith (in Figure S1) was marked as Chitosan/UiO-66-1 (the number 1 means the mass ratio of chitosan to UiO-66 is 1:1). The chitosan monolith without UiO-66 was also prepared using the similar procedure and was named Chitosan-M.

### 2.3. Adsorption experiments

A series of adsorption experiments were conducted to evaluate the adsorption properties of Chitosan/UiO-66-1, Chitosan-M and commercial activated carbon (AC) for CR. First, a stock solution of CR (1000 mg/L) was prepared by dissolving CR powder in ultrapure water and further diluted to the predetermined concentrations before use. The benchmark adsorption experiments were performed in glass bottles (with the size of  $\Phi$  22 mm  $\times$  50 mm) with 20 mg adsorbents (UiO-66 or Chitosan/UiO-66-1 or Chitosan-M) in 5 mL of CR solutions (50 mg/L, initial pH = 7.0) at 25 °C from 30 min to 1440 min. At a fixed time, the concentration of CR in the solution was measured using a UV-visible spectrophotometer (UV-1800 PC, Shanghai Meipuda instrument Co. Ltd., China). The specific adsorbed amount of CR was calculated according to the following equation:

$$q_t = \frac{(c_0 - c_t)}{m} V \quad (1)$$

where  $c_0$  (mg/L) is initial concentration of adsorbate,  $c_t$  (mg/L) is the concentration of adsorbate at time  $t$ ,  $m$  (g) is the mass of adsorbent,  $V$  (L) is the volume of the CR solution, and  $q_t$  (mg/g) is the CR amount adsorbed by the adsorbent at time  $t$ .

The adsorption isotherm experiments were performed via altering the CR initial concentration from 50 mg/L to 500 mg/L (5 mg adsorbent in 5 mL CR aqueous solution). In order to ensure the achievement of adsorption equilibrium, the adsorption continued for 24 h. For all experiments, CR solutions were always motionless (without stirring or shaking) during adsorption process. Before all adsorption tests, the calibration curve (Figure S2) of CR concentration vs. UV

absorbance at 490 nm was obtained using CR aqueous solutions with predeterminate concentration.

### 2.4. Material characterization

Nitrogen ( $N_2$ ) adsorption-desorption measurements were carried out using a Micromeritics ASAP 2020 HD88 system after pretreatment at 120 °C for 48 h. The specific surface areas, pore volumes and pore size distribution of UiO-66 powder and Chitosan/UiO-66-1 monolith were calculated by Brunauer-Emmett-Teller (BET) and Density Functional theory (DFT) methods. XRD patterns were acquired using an X-ray powder diffractometer with Cu anode (Bruker/D2), running at 40 kV and 30 mA, scanning from 5 to 70°. Before XRD evaluation, the chitosan/UiO-66 composite monolith was quenched using liquid nitrogen then pulverized. Morphologies of the samples were taken using a scanning electron microscope (SEM, VEGA 3SBU, Bruker). The samples were sputtered with a thin layer of Au prior to SEM imaging using plasma sputter instrument (JS-1600).

## 3. Results and discussion

### 3.1. Characterization of samples

In this work, UiO-66 particles were synthesized by solvothermal method successfully. The as-synthesized UiO-66 exhibits polygonal figuration as shown in Fig. 1B. When the mixture of UiO-66 and chitosan was crosslinked using glutaraldehyde and subsequently subjected to freezing and freeze-drying, the lamellar structures are observed in Fig. 1C. At higher magnification (Fig. 1D), it is clear that UiO-66 particles uniformly distribute on the surface of Chitosan/UiO-66-1, some embed in the chitosan pores wall and some just on the top surface (while surface of Chitosan-M is smooth as shown in Fig. 1A.). The similar morphology was also discerned in our previous work (freeze-drying chitosan/UiO-66 composite without GLA treatment) (Fu et al., 2017). This indicates that crosslinking by GLA may not change the morphology of the freeze-dried composite monolith obviously. In addition, in the previous work (Fu et al., 2017), in order to maintain the configuration of the freeze-dried monolith in water, the as-dried monoliths were washed in NaOH aqueous solution for remove HAc remaining in chitosan matrix; however, some UiO-66 particles were washed away in this procedure. In this work no obvious abscission of UiO-66 was observed.

The XRD patterns for the UiO-66 particles and Chitosan/UiO-66-1 are showed in Fig. 2. The diffraction peaks at  $2\theta = 7.1^\circ, 8.4^\circ, 11.9^\circ, 16.9^\circ, 22.1^\circ, 25.6^\circ, 30.6^\circ$  are corresponding to

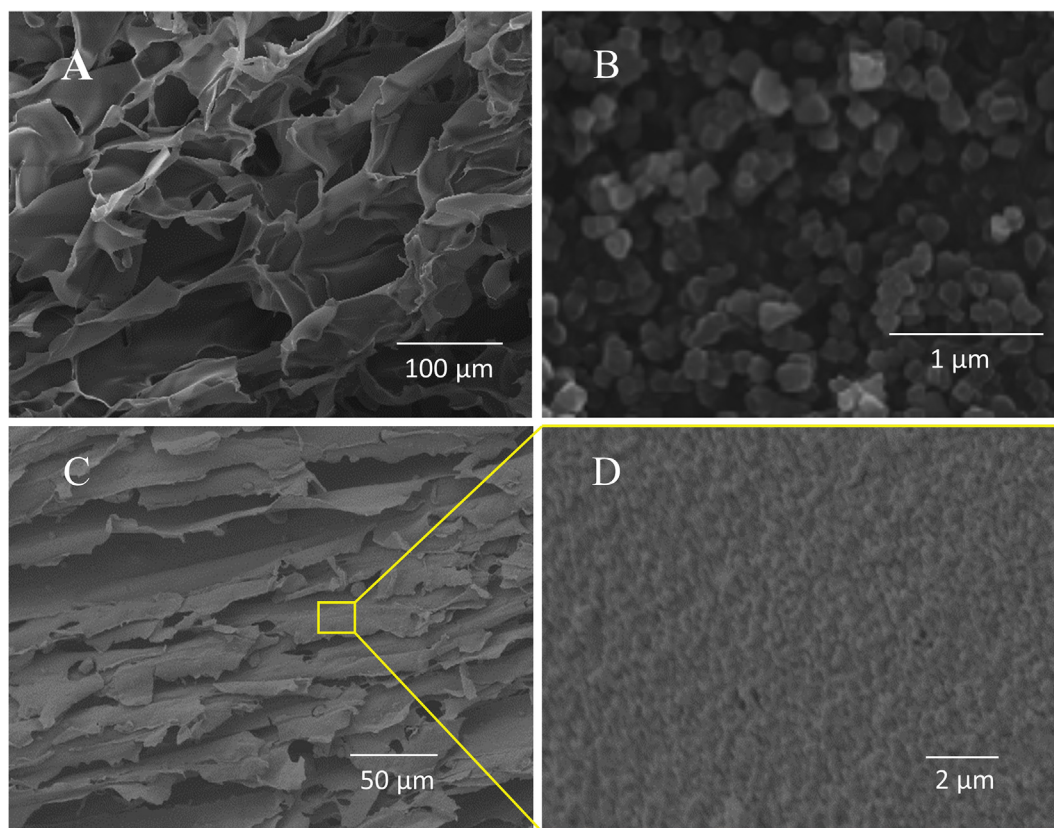


**Fig. 1** SEM images:(A) Chitosan-M, (B) UiO-66 nanoparticles, (C)&(D) Chitosan/UiO-66-1.

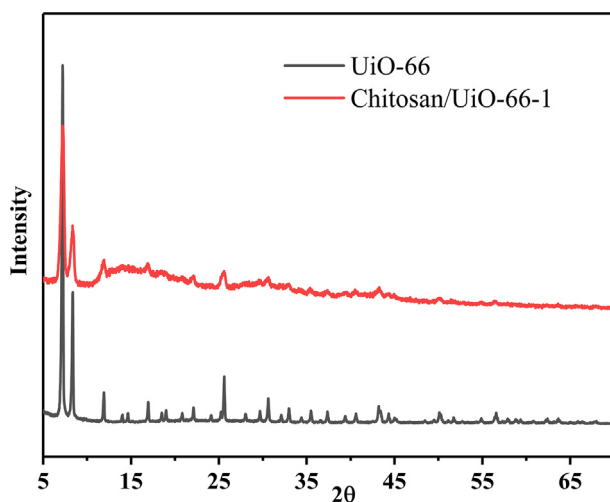


**Fig. 2** XRD patterns of UiO-66 and Chitosan/UiO-66-1.

UiO-66 (1 1 1), (0 0 2), (0 2 2), (0 0 4), (1 1 5), (2 2 4), (0 4 6) crystal planes, respectively, indicating UiO-66 was successfully synthesized (Cavka et al., 2008). Chitosan/UiO-66-1 shows the same main characteristic Bragg peaks, suggesting successful doping of UiO-66 in the composites without pronounced phase structure change, which is similar with the other research (Jin et al., 2018). Only some characteristic peaks are not quite

obvious, which may be caused by coating of glutaraldehyde and chitosan molecules on the surface of UiO-66.

The surface area of the obtained materials was evaluated through N<sub>2</sub> adsorption/desorption isotherms. The isotherms of UiO-66 (shown in Fig. 3A) is identified as typical type I, which is characteristic of microporous materials. Pore size distribution calculated using DFT theory confirms the existence of micropores (Fig. 3B). For Chitosan/UiO-66-1, the isotherm (Fig. 3A) slowly increases at low relative pressure suggesting the presence of mesopores. When relative pressure is close to 1, the isotherm appears to fast increase due to the presence of macropores. The pore size distribution of the composite monolith (Fig. 3B) demonstrates the co-existence of micro-, meso- and macro-pores. The special surface area was calculated using BET method. UiO-66 powder possesses a surface area of 1034 m<sup>2</sup>/g that is similar to the reported value (Valenzano et al., 2011). However, the special surface area of Chitosan/UiO-66-1 (122 m<sup>2</sup>/g) exhibits a large decrease compared with UiO-66 powder. This sharp decrease of BET surface was also reported in other MOF/polymer hybrids (Duan et al., 2019 Valenzano et al., 2011). The plausible reason is (1) chitosan matrix mainly contribute to mass but little to surface area (Fu et al., 2017), that is, 50% decrease of surface area may be caused by introduction of chitosan matrix; (2) glutaraldehyde molecules enter the inside or cover the surface of the UiO-66 particles, blocking the micro/mesopores; (3) the chitosan molecules encapsulate the UiO-66 nanoparticles, preventing them from contacting with adsorbates.

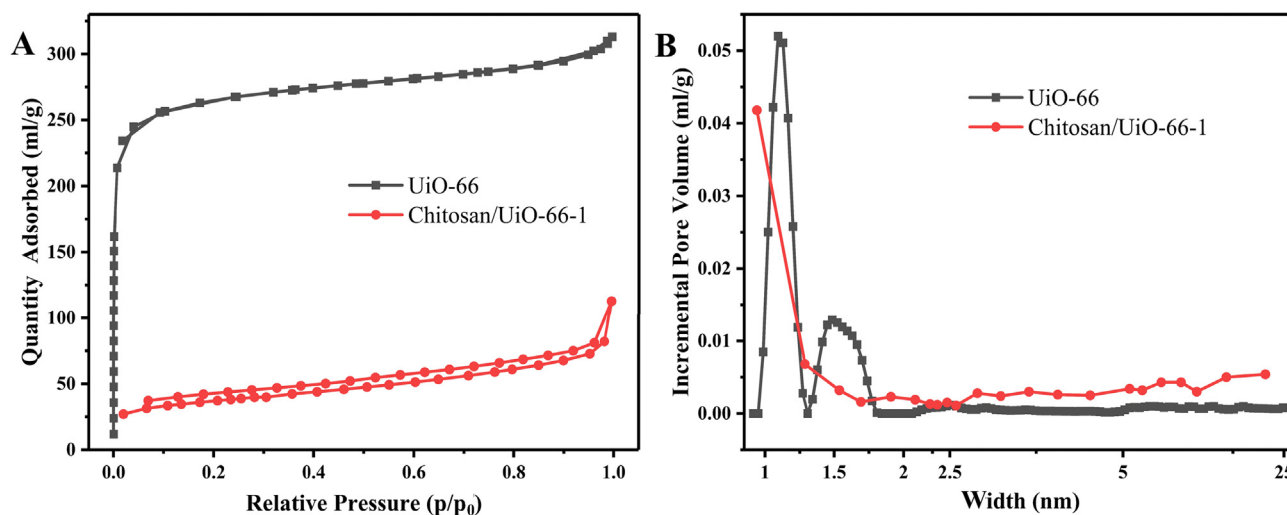


Fig. 3 (A) N<sub>2</sub> adsorption/desorption isotherms; (B) pore size distribution profiles.

### 3.2. Adsorption of CR

#### 3.2.1. Adsorption isotherms

In order to obtain the theoretical adsorption capacity and evaluate the adsorption isotherms, we carried out a set of benchmark adsorption experiments. The Langmuir and Freundlich models were also used to describe the adsorption data. The Langmuir isotherm can be expressed in linear form using the follows equation:

$$\frac{c_e}{q_e} = \frac{c_e}{q_{max}} + \frac{1}{q_{max}k_L} \quad (2)$$

where  $c_e$  is the equilibrium concentration of the solution (mg/L),  $q_{max}$  is the maximum adsorption capacity (mg/g),  $k_L$  is a Langmuir constant related to the affinity of the binding sites and energy of adsorption (L/mg). The curves of  $q_e - c_e$  are shown in

Fig. 4A. As it shows, equilibrium uptake increases with the rise of equilibrium CR concentration at the range of experimental concentrations. During adsorption, the higher concentration of adsorbate could provide the stronger driving force of solution, as a result, the active sites of adsorbent are surrounded by more adsorbate. Compared with Chitosan-M, UiO-66 and Chitosan/UiO-66-1 can easily achieve adsorptive equilibrium under relatively lower CR concentration, indicating UiO-66 in the hybrid plays a main role in CR adsorptive removal. The chitosan matrix also boosts the adsorption of CR because Chitosan/UiO-66-1 presents higher equilibrium adsorption capacity than UiO-66 at the same concentration. This phenomenon suggests, in static adsorption process, that chitosan matrix can support the UiO-66 particles avoiding the aggregation of the particles and decrease of active sites.

A linear relationship is obtained when  $c_e/q_e$  is plotted against  $c_e$  (Fig. 4 B), then  $q_{max}$  and  $k_L$  can be calculated from the slope and intercept. The relevant results are shown in Table 1. The coefficients of determination  $R^2 > 0.99$  means that the adsorption of CR on UiO-66, Chitosan/UiO-66-1 and Chitosan-M is consistent with Langmuir's model well, which indicates adsorption of CR on the three samples are monolayer and uniform adsorption. The maximum adsorption

capacities of the adsorbents were calculated according to Langmuir equation. The capacity is 246.91 mg/g for Chitosan/UiO-66-1, 199.2 mg/g for UiO-66 and 153.85 mg/g for Chitosan-M. It is worth noting that although the special surface area of Chitosan/UiO-66 is lower than UiO-66 (just around 1/9 that of UiO-66), the composite monolith substantiates the better adsorptive capacity than UiO-66, which indicates the BET surface is not the exclusive factor to determine the adsorption performance. Given the size of the CR molecule (~2.48 nm, in Figure S3), it cannot enter into the micropores (< 2 nm) of UiO-66. As such, the internal surface of micropores does not contribute to adsorption capacity. So, the CR molecules are mainly adsorbed on the external surface of the UiO-66 particles. By contrast, Chitosan/UiO-66-1 possesses meso- and macro-pores, which can provide plenty effective adsorptive sites for adsorption CR molecule.

In previous research UiO-66 can adsorb CR 283 mg/g (Han et al., 2018); however, the experimental value is only 169.56 mg/g adsorbed by UiO-66 in this work as shown in Table 2. There are two plausible reasons: (1) the UiO-66 particles in this work show lower mesoporous volume (0.047 cm<sup>3</sup>/g) than that of UiO-66 in previous work (0.06 cm<sup>3</sup>/g), so as to provide fewer available active sites for adsorption of CR; (2) static adsorption is employed in this work, compared to the static process oscillation can boost material transport onto MOFs particles.

There is another parameter  $R_L$ , which is dimensionless balance parameter. It can be used to determine whether the isotherm is favorable for adsorption: irreversible ( $R_L = 0$ ), favorable ( $0 < R_L < 1$ ), linear ( $R_L = 1$ ) or unfavorable ( $R_L > 1$ ).

$$R_L = \frac{1}{1 + k_L c_0} \quad (3)$$

where  $k_L$  (L/mg) is the Langmuir constant and  $c_0$  (mg/L) is the initial concentration of the solution. The changes of  $R_L$  values with  $c_0$  are shown in Fig. 4C. Despite of the change of initial concentrations (50 – 500 mg/L) of CR aqueous solution, the calculated  $R_L$  values are always in the range of 0 ~ 1, indicating the three adsorbents are favorable for adsorption of CR.

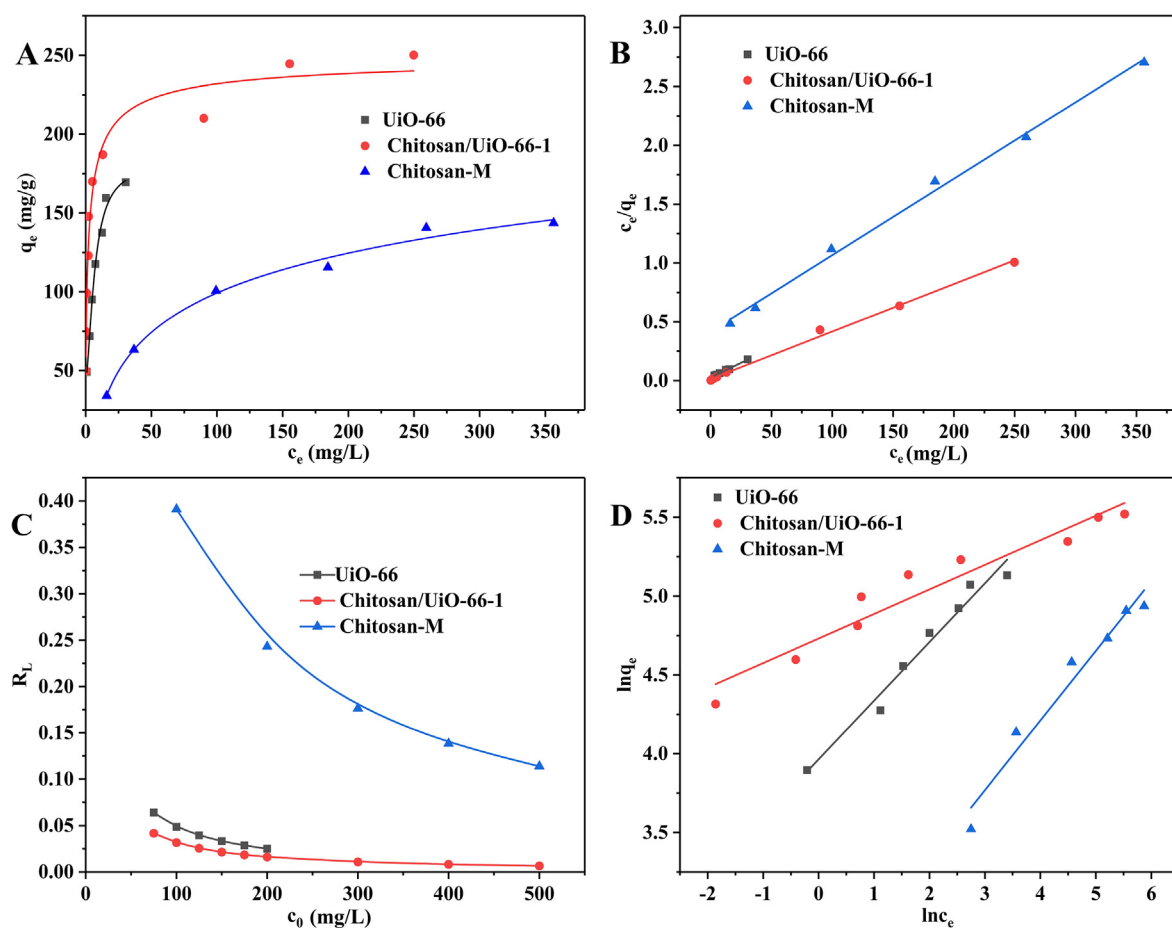


**Fig. 4** (A) Adsorption isotherms; (B) Langmuir isotherm plot; (C)  $R_L$  values at different initial concentrations of CR aqueous solution; (D) Freundlich isotherm plot.

**Table 1** Isotherm Parameters for the Adsorption of CR on Different Adsorbents.

	Langmuir			Freundlich			$q_{e,exp}$ (mg/g)
	$q_{max}$ (mg/g)	$K_L$ (L/mg)	$R^2$	$1/n$	$K_F$ (L/g)	$R^2$	
UiO-66	199.20	0.1951	0.996	0.3725	52.67	0.973	169.56
Chitosan/UiO-66-1	246.91	0.3063	0.997	0.1558	113.44	0.935	250.20
Chitosan-M	153.85	0.0156	0.996	0.4420	11.50	0.962	109.88

Note:  $q_{e,exp}$  is the experimental equilibrium adsorption capacity.

**Table 2** Comparison of CR adsorption capacities in this work and previous work.

sample	$q_{e,exp}$ (mg/g)	Adsorption method	Experimental Temperature (°C)	BET surface (m <sup>2</sup> /g)	
UiO-66	169.56	static	25	1034	This work
UiO-66	283.00	shaking	35	1358	(Han et al., 2018)
Chitosan/UiO-66-1	250.20	static	25	122	This work

The linear Freundlich isotherm equation is expressed as:

$$\ln q_e = \ln k_F + \frac{1}{n} \ln c_e \quad (4)$$

where  $k_F$  is a Freundlich constant related to adsorption capacity (L/g), the higher value of  $k_F$  indicates adsorption is feasible. The constant  $n$  is a measure of deviation from

linearity of the adsorption and usually used to verify types of adsorption. It is suggested that if  $1/n = 1$ , the adsorption is linear; further,  $1/n > 1$  indicates that adsorption may be a chemical process; whereas,  $1/n < 1$  is associated with a favorable adsorption and it also may have a physical process (Prabhu and Meenakshi, 2015; Dawood and Sen 2012; Vimonses et al., 2009). A straight line was obtained when  $\ln q_e$  was plotted against  $\ln c_e$  (Fig. 4D) and the values of  $1/n$  and  $k_F$  were calculated from the slope and intercept. The data are listed in Table 1. The values of  $1/n$  are between 0 and 1 for all samples, which confirms the samples are favorable for adsorbing CR molecules and some physical processes exist. Among the three adsorbents Chitosan/UiO-66-1 possesses the highest value of  $k_F$  indicating its best adsorptive performance.

### 3.2.2. Adsorption kinetics

The effect of time on the adsorption capacity of the three samples is shown in Fig. 5 A. When the initial CR concentration is 50 mg/L, the adsorption capacity of CR on the three samples increases fast during the first stage and then levels off after 60 min. The initial fast increase of adsorptive capacity is primarily caused by the abundant availability of active sites on the surface of the adsorbent (Bentahar et al., 2017; Huang et al., 2017). After a period of time, all active sites are gradually occupied by CR molecules leading to the decrease of

adsorption efficiency in the second stage (Dawood and Sen, 2012). The adsorbed quantities of CR over Chitosan/UiO-66-1 and UiO-66 are much higher (11.599 mg/g and 11.767 mg/g in 60 min, respectively) than that over AC (6.96 mg/g) in this study. During the process of adsorption, Chitosan/UiO-66-1 shows a high adsorptive effectiveness. The CR aqueous solution almost becomes absolute transparent after 90 min as shown in the inset photograph in Fig. 5A.

Adsorption kinetics was analyzed using Pseudo-first-order kinetics, Pseudo-second-order kinetic models and intraparticle diffusion model (Wang et al., 2007) to discover the adsorption mechanism. For Pseudo-first-order kinetics model, the adsorption rate is expected to be proportional to the first power of concentration, where the adsorption is characterized by diffusion through a boundary. Where Pseudo-second-order model assumes that chemisorption may be the rate-controlling step in the adsorption processes (Xu et al., 2019). The pseudo-first-order kinetic equation and the pseudo-second-order kinetic equation could be expressed with:

$$\log(q_e - q_t) = \log q_e - \frac{k_1}{2.303} t \quad (5)$$

$$\frac{t}{q_t} = \frac{1}{2k_2q_e^2} + \frac{t}{q_e} \quad (6)$$

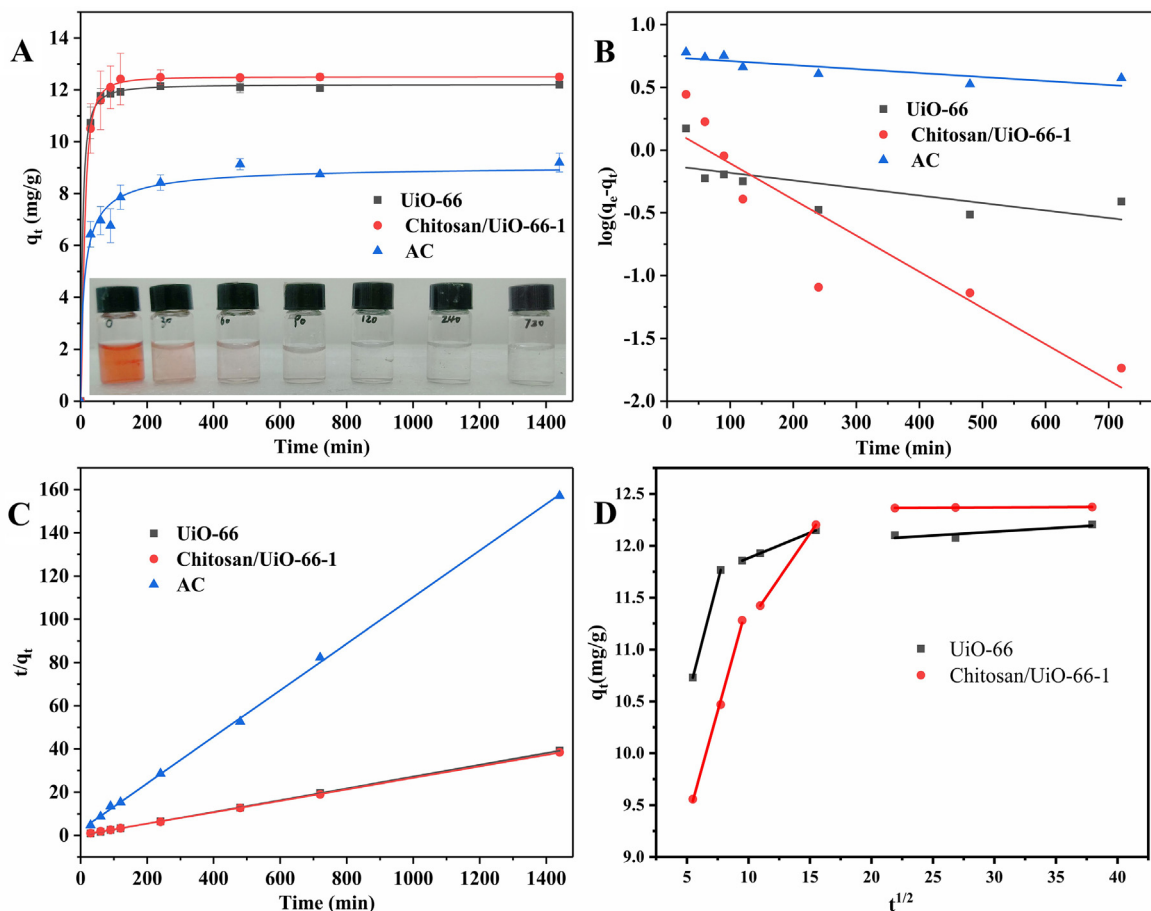


**Fig. 5** (A) Effects of time on adsorption capacity of UiO-66, Chitosan/UiO-66-1 and AC for CR. Adsorption experiments: concentration 50 mg/L; sample dosage: 20 mg in 5.00 mL; pH = 7.0; (B) Pseudo-first-order model; (C) Pseudo-second-order model; (D) intraparticle diffusion model.

where  $q_e$  (mg/g) is the adsorptive capacity at equilibrium,  $q_t$  (mg/g) is the amounts of dye adsorbed at time  $t$ ,  $k_1$  (1/min) and  $k_2$  (1/min) denote the rate constants of the pseudo-first-order and pseudo-second-order adsorption kinetics, respectively. With linear fitting procedures in Fig. 5B and C, the relevant parameters can be calculated on grounds of the equation (5) and (6), and the resultant values are summarized in Table 3. The correlation coefficients ( $R^2$ ) from pseudo-second-order adsorption kinetics are closer to 1, which means the adsorption of CR over the three adsorbents includes chemical adsorption (Xu et al., 2017).

Since neither the Pseudo-first-order nor the Second-order model can identify the diffusion mechanism, the kinetic results were analyzed by the intraparticle diffusion model to elucidate the diffusion mechanism whose model is expressed as:

$$q_t = k_i t^{1/2} \quad (7)$$

where  $k_i$  is the intraparticle diffusion rate constant (mg/g min<sup>1/2</sup>), which can be evaluated from the slope of the linear plot of  $q_t$  versus  $t^{1/2}$ . According to the intraparticle diffusion model, the relationship between the amount of dye adsorption ( $q_t$ ) and the square root of time ( $t^{1/2}$ ) should be linear. If these lines pass through the origin, then intraparticle diffusion is the only rate control step (Bhattacharyya and Sharma, 2005). However, as shown in Fig. 5D and in Table 4, these profiles are not linear over the entire time range. It can be divided into multi-linear curves, indicating that the adsorption process involves multiple stages, and intragranular transport is not a rate limiting step.

### 3.3. Recycling of adsorbents

The recovery and reusability of the adsorbent are very important for commercial and industrial applications. Although UiO-66 nanoparticle has been demonstrated to be high-performance adsorption for methyl orange and methylene blue, it is difficult to recover (Molavi et al., 2018). Generally, UiO-66 nanoparticle can only be collected by centrifugation or filtration (Molavi et al., 2018; He et al., 2014), which is a tedious process and will limit the upscale applications. To solve this issue, a MOF/polymer composite monolith (Chitosan/UiO-66-1) was fabricated to facilitate recycling of adsorbents in this work. As shown in Fig. 6A, the composite monolith can be taken out just by a pair of tweezers at the end of adsorption. It is clear that chitosan/UiO-66 composite monolith becoming red due to CR molecules attached on the monolith. This simple picking-up procedure can accelerate the recycling process for saving time and reducing energy consuming.

Chitosan/UiO-66-1 and UiO-66 powder were collected by picking out and centrifugation, respectively. Both the samples were washed sequentially with absolute ethanol (4 times, 30 min every time), acetone (3 times, 15 min per time), cyclohexane (3 times, 15 min per time), then were naturally air-dried for 48 h in a fume hood for the next cycle of adsorption experiment. The adsorptive uptake in 24 h ( $q_{24h}$ ) was used to observe their recycling adsorption capacity. As shown in Fig. 6 B, after four cycles, the values of  $q_{24h}$  of UiO-66 powder and Chitosan/UiO-66-1 are 8.815 mg/g and 11.497 mg/g, respectively. Chitosan/UiO-66-1 can retain over 90% adsorbed capacity of the fresh adsorbent, which demonstrates the composite monolith is a promising adsorbent for CR removal from water.

## 4. Conclusions

In this work, the chitosan/UiO-66 composite monolith was successfully prepared by ice templating method. Crosslinking procedure with GLA prevented the composite from dissolving in water, and did not change the typical ice-templated porous layered structure. Although the composite monolith presented a relatively low special surface area compared with UiO-66 powder due to plausible encapsulation of UiO-66 in chitosan and blockage of micropores, it still exhibited high adsorptive efficiency for CR from static wastewater. The chitosan/UiO-66 monolith can remove almost all CR from 50 mg/L CR aqueous solution within 90 min. This suggests the chitosan matrix can make active sites on UiO-66 contact with adsorbates enough by holding up the particles, avoiding their overlapping. Furthermore, the method of preparing composite monolith provides a facile recycling method. These merits make it a promising adsorbent for dyes adsorption removal.

## Acknowledgement

The work was supported by National Natural Science Foundation of China (51902216), Foundation of Sichuan Provincial Department of Education (Grants 18ZA0351), Project of Science and Technology Department in Sichuan province (Grants 2018JY0493), Foundation of Introduced Talent of Sichuan University of Science and Engineering (Grants 2017RCL27), Foundation of Key Laboratory of Automobile High Performance Materials and Forming Technology of Sichuan Province (Grants SZJJ2017-017) and Innovation Fund for Postgraduate of Sichuan University of Science and Engineering (Grants y2018047).

**Table 3** Parameters of pseudo-first-order and pseudo-second-order kinetic models.

sample	Pseudo-first-order				Pseudo-second-order		
	$q_{e,exp}$ (mg/g)	$K_1$ (1/min)	$q_e$ (mg/g)	$R^2$	$K_2$ (1/min)	$q_e$ (mg/g)	$R^2$
UiO-66	12.205	$7.23 \times 10^{-4}$	0.66	0.4203	0.0045	36.76	1
Chitosan/UiO-66-1	12.499	$3.39 \times 10^{-7}$	1.25	0.6843	0.0020	37.75	0.9999
AC	9.197	$4.00 \times 10^{-7}$	5.16	0.6324	0.0039	9.28	0.9994

**Table 4** Parameters of intraparticle diffusion model.

sample	$k_1$ (mg/g min <sup>1/2</sup> )	$R^2$	$k_2$ (mg/g min <sup>1/2</sup> )	$R^2$	$k_3$ (mg/g min <sup>1/2</sup> )	$R^2$
UiO-66	0.45674	1	0.04863	0.9999	0.00731	0.76897
Chitosan/UiO-66-1	0.42793	0.99822	0.1717	1	0.00059	0.95693

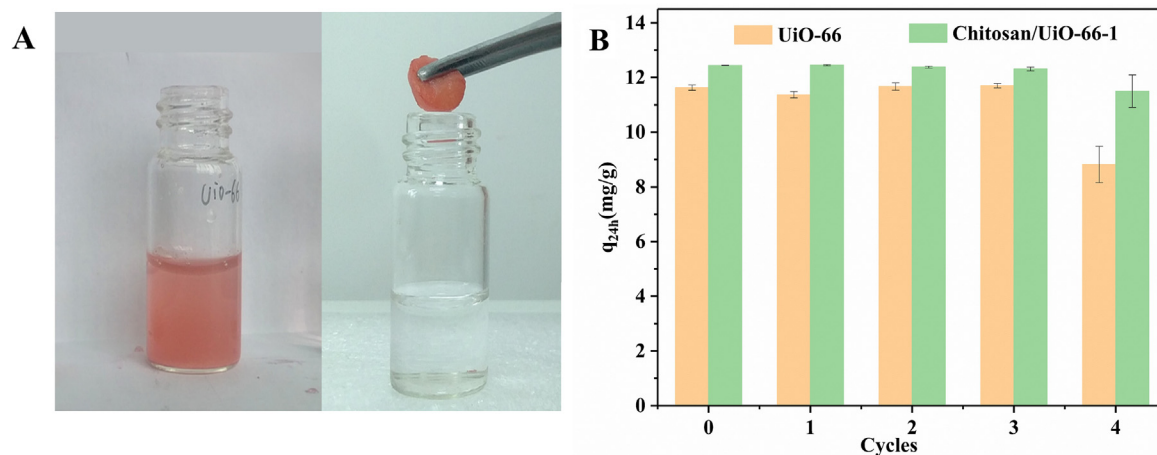


**Fig. 6** (A) Digital picture of UiO-66 (left) and Chitosan/UiO-66-1(right) during recycling, and the latter can be taken out by a simple picking-up; (B) reusability of UiO-66 and Chitosan/UiO-66-1 for the adsorptive removal of CR from 5 mL of 50 mg/L CR aqueous solution.

## Appendix A. Supplementary data

Supplementary data to this article can be found online at <https://doi.org/10.1016/j.arabjc.2020.04.007>.

## References

- Ahmed, I., Jhung, S.H., 2014. *Mater. today* 17, 136–146.
- Ahmed, I., Khan, N.A., Jhung, S.H., 2017. *Chem. Eng. J.* 321, 40–47.
- Beheshti, A., Nozarian, K., Ghamari, N., Mayer, P., Motamedi, H., 2018. *J. Solid State Chem.* 258, 618–627.
- Bentahar, S., Dbik, A., El Khomri, M., El Messaoudi, N., Lacherai, A., 2017. *J. Environ. Chem. Eng.* 5, 5921–5932.
- Bhatt, A.S., Sakaria, P.L., Vasudevan, M., Pawar, R.R., Sudheesh, N., Bajaj, H.C., Mody, H.M., 2012. *RSC adv.* 2, 8663–8671.
- Bhattacharyya, K.G., Sharma, A., 2005. *Dyes pigments.* 65, 51–59.
- Bulut, E., Özacar, M., Şengil, İ.A., 2008. *J. Hazard. Mater.* 154, 613–622.
- Cavka, J.H., Jakobsen, S., Olsbye, U., Guillou, N., Lamberti, C., Bordiga, S., Lillerud, K.P., 2008. *J. Am. Chem. Soc.* 130, 13850–13851.
- Chakraborty, S., Purkait, M.K., DasGupta, S., De, S., Basu, J.K., 2003. *Sep. Purif. Technol.* 31, 141–151.
- Chatterjee, S., Lee, D.S., Lee, M.W., Woo, S.H., 2009. *Bioresource Technol.* 100, 2803–2809.
- Chen, Q., He, Q., Lv, M., Xu, Y., Yang, H., Liu, X., Wei, F., 2015. *Applied Surface Science.* 327, 77–85.
- Chen, R., Wang, W., Zhao, X., Zhang, Y., Wu, S., Li, F., 2014. *Chem. Eng. J.* 242, 226–233.
- Dawood, S., Sen, T.K., 2012. *Water Res.* 46, 1933–1946.
- Deville, S., 2018. *Scripta Mater.* 147, 119–124.
- Du, Q., Li, Y., Li, J., Zhang, Z., Qiao, B., Sui, K., Wang, D., Wang, C., Li, H., Xia, Y., 2019. *International Journal of Nanoscience.* 18, 1850030.
- Duan, P., Moreton, J.C., Tavares, S.R., Semino, R., Maurin, G., Cohen, S.M., Schmidt-Rohr, K., 2019. *J. Am. Chem. Soc.* 141, 7589–7595.
- Fan, X., Yu, L., Li, L., Yang, C., Wen, J., Ye, X., Cheng, J., Hu, Y., 2017. *Mater. Res. Express* 4, 026404.
- Frid, P., Anisimov, S.V., Popovic, N., 2007. *Brain Res. Rev.* 53, 135–160.
- Fu, Q., Wen, L., Zhang, L., Chen, X., Pun, D., Ahmed, A., Yang, Y., Zhang, H., 2017. *ACS appl. Mater. Inter.* 9, 33979–33988.
- Fu, Q., Wen, L., Zhang, L., Chen, X., Zhang, H., 2019. *Ind. Eng. Chem. Res.* 58, 14312–14322.
- Gupta, V.K., Kumar, R., Nayak, A., Saleh, T.A., Barakat, M.A., 2013. *Adv. Colloid. interfac.* 193, 24–34.
- Han, W., Jiang, Z., Yan, W., Hua, Z., Wang, Y., 2018. *J. Clean. Prod.* 188, 575–588.
- Han, Y., Liu, M., Li, K., Sun, Q., Zhang, W., Song, C., Zhang, G., Zhang, Z.C., Guo, X., 2017. *Front.* 4, 1870–1880.
- He, Q., Qi, C., Lü, M., Liu, X., 2014. *Chinese J. Chem. Eng.* 22, 1285–1290.
- He, X., Male, K.B., Nesterenko, P.N., Brabazon, D., Paull, B., Luong, J.H.T., 2013. *ACS Appl. Mater. inter.* 5, 8796–8804.
- Huang, D., Deng, R., Wan, J., Zeng, G., Xue, W., Wen, X., Zhou, C., Hu, L., Liu, X., Xu, Piao, Guo, X., Ren, X., 2018. *J. Hazard. Mater.* 348, 109–116.
- Huang, Z., Li, Y., Chen, W., Shi, J., Zhang, N., Wang, X., Li, Z., Gao, L., Zhang, Y., 2017. *Mater. Chem. Phys.* 202, 266–276.
- Jin, P., Tan, W., Huo, J., Liu, T., Liang, Y., Wang, S., Bradshaw, D., 2018. *J. Mater. Chem. A* 6, 20473–20479.
- Kalaj, M., Denny Jr, M.S., Bentz, K.C., Palomba, J.M., Cohen, S.M., 2019. *Angew. Chem. Inter. Ed.* 58, 2336–2340.
- Kalantari, K., Afifi, M.A., 2018. *Sep. Sci. Technol.* 53, 2527–2535.

- Kumar, S., Verma, G., Gao, W.Y., Niu, Z., Wojtas, L., Ma, S., 2016. *Eur. J. Inorg. Chem.* 2016, 4373–4377.
- Lai, K.C., Lee, L.Y., Hiew, B.Y.Z., Thangalazhy-Gopakumar, S., Gan, S., 2018. *J. Environ. Sci.*
- Li, S., Chen, Y., Pei, X., Zhang, S., Feng, X., Zhou, J., Wang, B., 2016. *Chinese J. Chem.* 34, 175–185.
- Lim, G.J.H., Wu, Y., Shah, B.B., Koh, J.J., Liu, C.K., Zhao, D., Cheetham, A.K., Wang, J., Ding, J., 2019. *ACS Materials Letters.* 1, 147–153.
- Lin, K.-Y.A., Liu, Y.-T., Chen, S.-Y., 2016. *J. Colloid. interfac.* 461, 79–87.
- Lv, S.-W., Liu, J.-M., Ma, H., Wang, Z.-H., Li, C.-Y., Zhao, N., Wang, S., 2019. *Mat.* 282, 179–187.
- Ma, J., Guo, X., Ying, Y., Liu, D., Zhong, C., 2017. *Chem. Eng. J.* 313, 890–898.
- Maurin, G., Serre, C., Cooper, A., Férey, G., 2017. *Chem. Soc. Rev.* 46, 3104–3107.
- Mittal, H., Kumar, V., Alhassan, S.M., Ray, S.S., 2018. *Int. J Biol macromol.* 114, 283–294.
- Mohammadnejad, M., Hajiashrafi, T., Rashnavadi, R., 2017. *J. Porous Mat.* 25, 1–9.
- Molavi, H., Hakimian, A., Shojaei, A., Raeiszadeh, M., 2018. *Appl. Surf. Sci.* 445, 424–436.
- Oveisi, M., Asli, M.A., Mahmoodi, N.M., 2017. *J. Hazard. Mater.* 347, 123–140.
- Park, J., Wang, Z.U., Sun, L.-B., Chen, Y.-P., Zhou, H.-C., 2012. *J. Am. Chem. Soc.* 134, 20110–20116.
- Prabhu, S.M., Meenakshi, S., 2015. *Desalin. Water Treat.* 53, 3592–3603.
- Puvaneswari, N., Muthukrishnan, J., Gunasekaran, P., 2006. *Indian. J. Exp. Biol* 44, 618–626.
- Roleček, J., Pejchalová, L., Martínez-Vázquez, F.J., González, P.M., Salamon, D., 2019. *J. Eur. Soc.* 39, 1595–1602.
- Salleh, M.A.M., Mahmoud, D.K., Karim, W.A.W.A., Idris, A., 2011. *Desalination.* 280, 1–13.
- Seo, Y.S., Khan, N.A., Jhung, S.H., 2015. *Chem. Eng. J.* 270, 22–27.
- Shetti, N.P., Malode, S.J., Malladi, R.S., Nargund, S.L., Shukla, S.S., Aminabhavi, T.M., 2019. *Microchem. J.* 146, 387–392.
- Suresh, K., Kumaraswamy, G., 2019. *J. Phys. D. Appl. Phys.* 52, 214002.
- Tian, C., Feng, C., Wei, M., Wu, Y., 2018. *Chemosphere* 208, 476–483.
- Valenzano, L., Civalleri, B., Chavan, S., Bordiga, S., Nilsen, M.H., Jakobsen, S., Lillerud, K.P., Lamberti, C., 2011. *Chem. Mater.* 23, 1700–1718.
- Vimonses, V., Lei, S., Jin, B., Chow, C.W.K., Saint, C., 2009. *Chem. Eng. J.* 148, 354–364.
- Wang, L., Wang, A.q., 2007. *Clean Technol.* 82, 711–720.
- Xu, D., Cao, J., Li, Y., Howard, A., Yu, K., 2019. *Waste Manage.* 87, 652–660.
- Xu, S., Lv, Y., Zeng, X., Cao, D., 2017. *Chem. Engin. J.* 323, 502–511.
- Xue, W., Huang, D., Zeng, G., Wan, J., Zhang, C., Xu, R., Cheng, M., Deng, R., 2018. *J. Hazard. Mater.* 341, 381–389.
- Zhao, C., Zheng, H., Sun, Y., Zhang, S., Liang, J., Liu, Y., An, Y., 2018a. *Sci. Total. Environ.* 640, 243–254.
- Zhao, X., Wang, Y., Li, D.S., Bu, X., Feng, P., 2018b. *Adv. Mater.* 30, 1705189.